Journal of Power Sources 195 (2010) 374–379

Contents lists available at ScienceDirect

Journal of Power Sources

journal homepage: www.elsevier.com/locate/jpowsour

Effect of Mg_3MnNi_2 on the electrochemical characteristics of Mg_2Ni electrode alloy

Fu-Kai Hsu [a], Chih-Kuang Lin [a], Sheng-Long Lee [b,*], Chun-Yu Lin [c], Hui-Yun Bor [d]

[a] Department of Mechanical Engineering, National Central University, Jhongli, Taiwan
[b] Institute of Materials Science and Engineering/Department of Mechanical Engineering, National Central University, No. 300, Jhongda Rd., Jhongli 32001, Taiwan
[c] Institute of Materials Science and Engineering, National Central University, Jhongli, Taiwan
[d] Materials Research and Electro-Optics Division, Chung-Shan Institute of Science and Technology, Longtan, Taiwan

ARTICLE INFO

Article history:
Received 23 March 2009
Received in revised form 9 July 2009
Accepted 11 July 2009
Available online 21 July 2009

Keywords:
Composite hydrogen storage alloy
Isothermal evaporation casting process
Electrochemical characteristics

ABSTRACT

Mg_2Ni–x mol% Mg_3MnNi_2 (x = 0, 15, 30, 60, 100), the novel composite alloys employed for hydrogen storage electrode, have been successfully synthesized by a method combining electric resistance melting with isothermal evaporation casting process (IECP). X-ray diffraction (XRD) analysis results show that the composite alloys are composed of Mg_2Ni phases and the new Mg_3MnNi_2 phases. It is found on the electrochemical studies that maximum discharge capacities of the composite alloys increase with the increasing content of the Mg_3MnNi_2 phase. The discharge capacity of the electrode alloy is effectively improved from 17 mAh g^{-1} of the Mg_2Ni alloy to 166 mAh g^{-1} of the Mg_3MnNi_2 alloy. Among these alloys, the Mg_3MnNi_2 phase possesses a positive effect on the retardation of cycling capacity degradation rate of the electrode materials. Cyclic voltammetry (CV) results confirm that the increasing content of the Mg_3MnNi_2 phase effectively improves the reaction activity of the electrode alloys. Surface analyses indicate that the Mg_3MnNi_2 phase can enhance the anti-corrosive performance of the particle surface of these composite alloys.

1. Introduction

Mg-based hydrogen storage alloys are considered as the negative electrode materials for nickel–metal hydride (Ni–MH) batteries because of their high theoretical discharge capacity, light weight, low cost and abundant resources [1]. However, their rapid capacity decay in KOH electrolyte limited the practical application of Mg-based alloys to Ni–MH battery systems. In order to improve the electrode performance of Mg_2Ni alloy, modification of its composition by partial substitution of Mg and/or Ni has been widely studied [2–6]. It was found that Mn as partial substitute for Mg or Ni in Mg_2Ni alloys was effective in increasing the electrode cycle life [2–5]. Mg_2Ni-based alloys containing the Mg_3MnNi_2 phase of the cubic crystal structure could restrain the alloy surface from corrosion in alkaline solution [5]. It was reported by Denys et al. [7] that new intermetallic compound Mg_3MnNi_2 also exhibited an ideal discharge capacity and good cyclic stability in comparison with other Mg-based alloys.

Most of hydrogen storage materials with the nanocrystalline structure have been widely prepared by the method combining mechanical alloying with the annealing or sintering procedure [2–4,7]. However, it usually takes a longer time to prepare alloy by the mechanical alloying method and the homogeneous sample is difficult to obtain. Besides, the impurity could be introduced into the desired composition during the milling process [8]. An innovative method integrating conventional melting and isothermal evaporation casting process (IECP) has been proposed to produce the Mg_2Ni alloy. It was reported [9] the attractive characteristics of this method was used on the mass production of highly pure and homogeneous Mg_2Ni alloy.

In spite of some studies on improving the electrochemical characteristics of Mg_2Ni alloy through manganese addition [2–6], few ones on the surface analyses of modified alloy electrode were performed. Therefore, the composite alloys Mg_2Ni–x mol% Mg_3MnNi_2 (x = 0, 15, 30, 60, 100) have been synthesized by the method combining electric resistance melting with IECP. The influence of the Mg_3MnNi_2 phase on the structure, surface chemical composition and electrochemical properties of the synthesized materials was studied. These measurements may supply useful information over the anti-corrosion performance on the surface of the studied materials.

2. Experimental

Section 3 will detail the concept and the procedure to prepare the composite alloys Mg_2Ni–x mol% Mg_3MnNi_2 (x = 0, 15, 30, 60,

* Corresponding author. Tel.: +886 3 4267325; fax: +886 3 4254501.
E-mail address: shenglon@cc.ncu.edu.tw (S.-L. Lee).

0378-7753/$ – see front matter © 2009 Elsevier B.V. All rights reserved.
doi:10.1016/j.jpowsour.2009.07.020

100). To confirm the purity of the composite alloys, the structure and composition were examined by X-ray diffraction (XRD) and inductively coupled plasma-atomic emission spectroscopy (ICP-AES). The bulk sample was mechanically ground to 2000 grade SiC paper and polished to 0.05 μm Al_2O_3 powders before microstructure observation. Then, the surface morphology and atomic ratio of the composite alloys were investigated with the scanning electron microscopy (SEM) and the electron probe X-ray microanalyzer (EPMA). In order to determine the freezing point of the Mg_3MnNi_2 phase, a pure Ar flow was induced into the differential scanning calorimeter (DSC) heated from 25 to 1200 °C at a rate of 10 °C min^{-1}. The constituent elements of the surface of the composite alloys were examined with X-ray photoelectron spectroscopy (XPS) depth profiles after cycle life testing. Accelerated Ar^+ ions at 3.0 keV were sputtered on the alloy surface at a rate of ca. 1.0 Å s^{-1}.

Electrochemical charge and discharge cycling tests were performed with a Neware battery test system, employing a two-electrode cell in 6 M KOH and 1 wt% LiOH electrolyte at room temperature. The working electrode was fabricated in the following procedure. The mixture that was composed of 1 g composite materials, 2 g nickel powders and 0.01 g polyvinyl alcohol solution was pasted onto both sides of the foam nickel sheet, which was previously spot-weld onto a nickel wire. The mixture pasted onto foam nickel, after being dried, was cold pressed at 40 MPa. The counter electrode was $NiOOH/Ni(OH)_2$. The working electrode was charged at 50 mA g^{-1} for 10 h and discharged at 10 mA g^{-1} with a cut-off potential set at 1.0 V. The resting time between charge and discharge was 10 min.

The cyclic voltammetry (CV) curves were measured with a CH/600C instrument in a three-electrode system with the composite alloys as working electrode, a platinum as counter electrode and Hg/HgO as reference electrode. The scan rate of CV measurement was 5 mV s^{-1} and the scan range was between −1.2 and −0.35 V.

3. Results and discussion

3.1. The concept and procedure of alloy fabrication

The primary Mg_3MnNi_2 alloy could be formed first at around 1120 °C according to DSC analysis and the final products would be the mixture of Mg_3MnNi_2, Mg_2Ni and Mg, respectively. The primary and eutectic reactions based on the Mg–Ni binary phase diagram took place during the cooling process because the electric resistance melting of Mg, Ni and Mn elements was adopted. Reaction Eq. (1) was as follows:

$$(3x+2y+z)Mg_{(l)}+xMn_{(l)}+(2x+y)Ni_{(l)} \rightarrow xMg_3MnNi_{2(s)}+yMg_2Ni_{(s)}+zMg_{(s)} \quad (1)$$

This experiment intends to produce the composite alloys Mg_2Ni–x mol% Mg_3MnNi_2 with various Mg_3MnNi_2 contents. Therefore, reaction Eq. (2) is acquired through modifying reaction Eq. (1) by adjusting the proportion of Mg, Ni and Mn elements and utilizing IECP to evaporate the Mg element.

Suppose $z = 0$, $y = 1 - x$ from Eq. (1):

$$(x+2)Mg_{(l)}+xMn_{(l)}+(x+1)Ni_{(l)} \rightarrow xMg_3MnNi_{2(s)}+(1-x)Mg_2Ni_{(s)} \quad (2)$$

When the nominal composition of 15 mol% Mg_3MnNi_2–85 mol% Mg_2Ni, i.e. 40.8 Mg–52.7 Ni–6.5 Mn (wt%) was applied to prepare the MMN15 alloy, an unexpected $MgNi_2$ phase would be produced. To avoid the formation of $MgNi_2$ phase, an excess amount of Mg was added to change the weight ratio of Mg and Ni in the Mg–Ni phase within an appropriate range after formation of the primary Mg_3MnNi_2 phase. According to the binary Mg–Ni phase diagram, the appropriate wt% of Ni to produce Mg_2Ni phase is between 23.5 and 49.7. Therefore, a modified composition 50.3 Mg–44.3 Ni–5.4 Mn (wt%) was employed for the raw materials to make the MMN15 alloy. The thermal profile of the MMN15 alloy prepared by the method combining electric resistance melting with IECP is illustrated in Fig. 1. There are three main steps: Mg–Mn–Ni melting and mixing, primary Mg_3MnNi_2 alloy formation and Mg_2Ni alloy purifying.

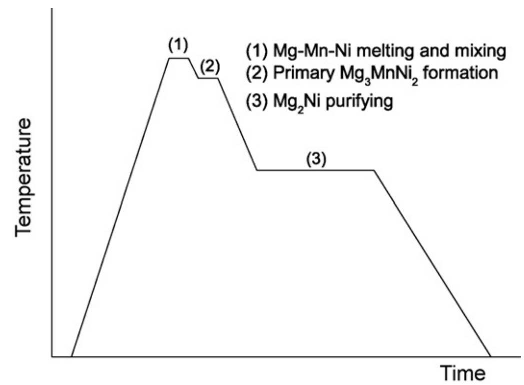

Fig. 1. The thermal profile of the MMN15 (15 mol% Mg_3MnNi_2–85 mol% Mg_2Ni) alloy preparing.

(1) Mg–Mn–Ni melting and mixing: Mg bulks prepared from commercial pure Mg ingot (99.9 wt% purity) without cutting oil, commercial fine Mn powder (<75 μm, 99.9 wt% purity) and Ni powder (<10 μm, 99.99 wt% purity) were used in this work. A weight of 160 g mixture of Mg bulk, Mn powder and Ni powder with the composition of 50.3 Mg–44.3 Ni–5.4 Mn (wt%) was prepared as raw materials for the preparation of the MMN15 alloy. The raw materials were put into a stainless steel crucible (diameter 10 cm × 25 cm) and heated by an electric resistance furnace under an argon atmosphere at 1200 °C for 0.5 h. The homogeneous Mg–Mn–Ni liquid phase was easily obtained at 1200 °C by continuous stirring.
(2) Primary Mg_3MnNi_2 alloy formation: after the homogeneous Mg–Mn–Ni liquid formation, the well-mixed melt was cast into a preheated thin plate mold and held at 1120 °C for 0.5 h to obtain primary Mg_3MnNi_2 alloy. The proportion of primary Mg_3MnNi_2 alloy and liquid phase was affected by the holding temperature and the composition of the raw materials. When the Mg_3MnNi_2 alloy was composed of 7.2 wt% Mg, 5.4 wt% Mn and 11.6 wt% Ni, and produced at 1120 °C, the un-reactive composition of 56.9 wt% Mg–43.1 wt% Ni still existed in the liquid phase.
(3) Mg_2Ni alloy purifying: after the primary Mg_3MnNi_2 alloy formation, the homogeneous Mg–Ni liquid was cooled and held at 750 °C for 3.0 h to accelerate the evaporation of the excess Mg in the liquid phase. With the decrease of Mg, the composition of liquid phase would gradually shift to the Ni-rich direction and end at the theoretical composition of Mg_2Ni alloy based on the Mg–Ni phase diagram.

Eventually, the mixture of primary Mg_3MnNi_2 and Mg_2Ni alloy was left. The characteristic of synthesizing the composite alloys Mg_2Ni–x mol% Mg_3MnNi_2 with various Mg_3MnNi_2 contents could be applied to both formation proportions of Mg_3MnNi_2 through adding Mn element and Mg_2Ni alloy synthesis through IECP.

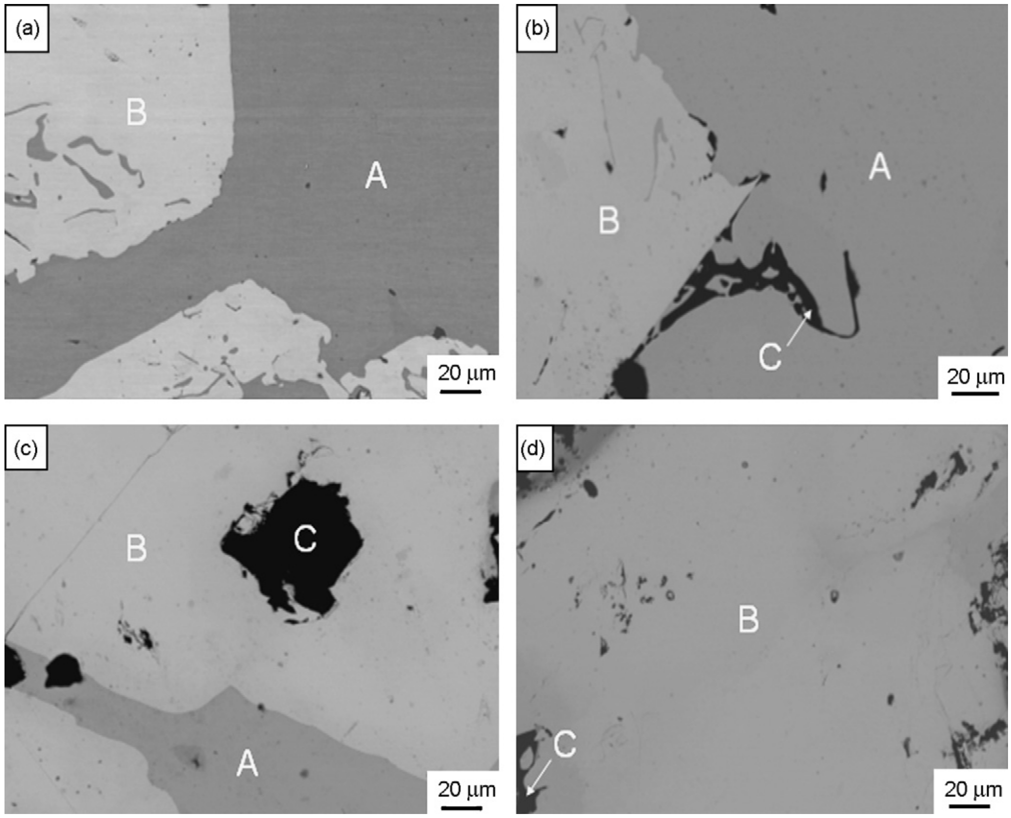

Fig. 2. SEM images of the as-cast alloys: (a) MMN15, (b) MMN30, (c) MMN60 and (d) MMN100 (A: Mg_2Ni with Mn solute atoms, B: Mg_3MnNi_2 and C: porosity).

3.2. The microstructure of the as-cast alloys

The observations on the microstructure of the composite alloys MMN*X* (*X* represents Mg_3MnNi_2 content in the composite alloy) are shown in Fig. 2. According to EPMA analysis, the A region signifies Mg_2Ni alloy with few Mn solute atoms and its atomic ratio is nearly 65.9 Mg, 31.9 Ni and 2.2 Mn in Fig. 2(a)–(c). EPMA indicates the B region is Mg_3MnNi_2 alloy with a similar atomic ratio of 49.6 Mg, 34.6 Ni and 15.8 Mn, which is close to the ideal ratio of 50 Mg, 33.3 Ni and 16.7 Mn in Fig. 2(a)–(d). The C regions are deep porosities caused by the loss of Mg during the evaporation procedure. With the increase of the Mg_3MnNi_2 phase, the microstructure of the composite alloys turns gradually from two phases to single phase.

Fig. 3 shows the X-ray diffraction patterns of the composite alloys MMN*X* with various Mg_3MnNi_2 contents. All diffraction peaks of MMN0 alloy correspond to the JCPDS 75-1250 standards of Mg_2Ni alloy in Fig. 3(a). In Fig. 3(b), it was also found that a new phase, Mg_3MnNi_2, was formed in the MMN15 alloy according to the SEM analysis. With the rise of Mg_3MnNi_2 contents, the amount of the Mg_2Ni phase gradually decreases and the relative amount of the new phase gradually increases. Fig. 3(e) shows that, when the Mg_3MnNi_2 concentration reaches $x = 100$, the Mg_2Ni phase almost disappears. It was found that only single phase Mg_3MnNi_2 was formed in the MMN100 alloy, which echoed the result of the SEM analysis. In addition, Table 1 demonstrates the impurity amount of as-cast alloys evaluated with ICP-AES identification. Except for few amounts of Cr, Fe and O, the analytic compositions of as-cast alloys are close to the theoretical compositions of the composite alloys.

According to the identification of SEM and ICP-AES, the pure and homogeneous Mg_3MnNi_2 alloy would be successfully fabricated by electric resistance melting of Mg, Ni and Mn element. In order to determine the freezing point of the Mg_3MnNi_2 phase, DSC analysis of a pallet-type one is carried out at the temperature range from 25 to 1200 °C. The resulting profile is shown in Fig. 4. An endothermic peak can be observed at around 1120 °C after melting of the alloy powder.

3.3. Discharge performance

The effects of the electrode alloys with various Mg_3MnNi_2 contents on the discharge behavior are shown in Fig. 5. The dis-

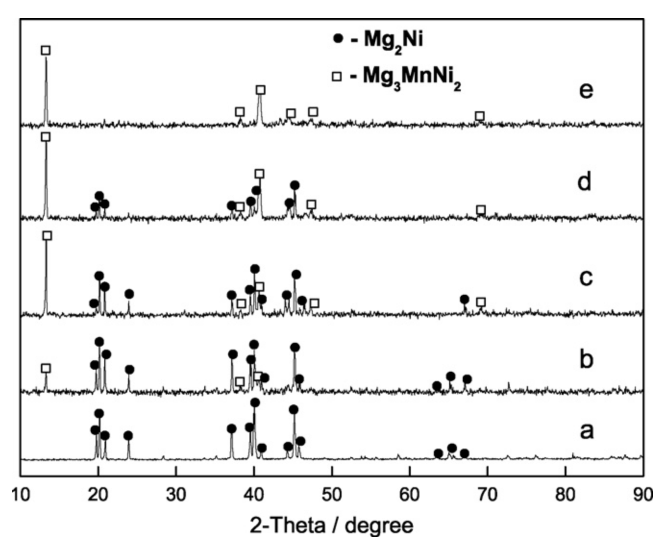

Fig. 3. XRD patterns of the as-cast alloys: (a) MMN0, (b) MMN15, (c) MMN30, (d) MMN60 and (e) MMN100.

Table 1
The ICP-AES identification of the as-cast MMNX ($0 \leqq X \leqq 100$) alloys.

Alloys	Theoretical composition (wt%)			Real composition (wt%)					
	Mg	Ni	Mn	Mg	Ni	Mn	Fe	Cr	O
MMN0	45.3	54.7	0	45.7	53.9	0.02	0.3	0.03	0.04
MMN15	40.8	52.7	6.5	41.2	52.2	6.2	0.31	0.03	0.05
MMN30	37.6	51.3	11.1	38.1	50.7	10.8	0.32	0.02	0.05
MMN60	33.3	49.4	17.3	33.6	48.9	17.1	0.3	0.03	0.06
MMN100	29.7	47.9	22.4	30.0	47.5	22.1	0.31	0.02	0.06

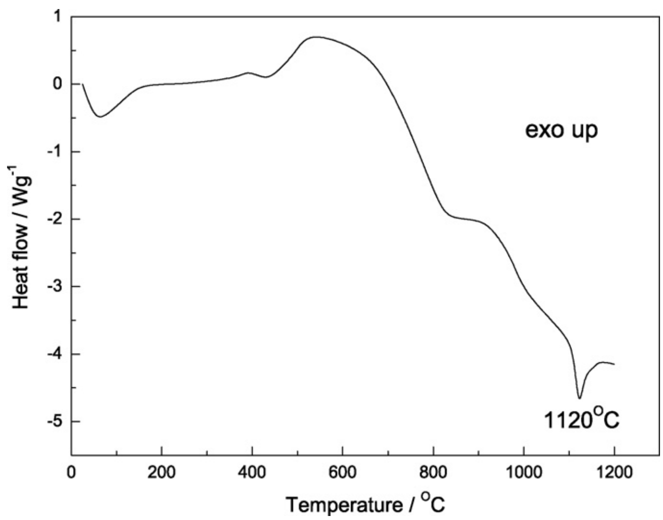

Fig. 4. DSC profile of the as-cast Mg_3MnNi_2 alloy (the endothermic peak around 1120 °C indicated the melt of Mg_3MnNi_2 alloy).

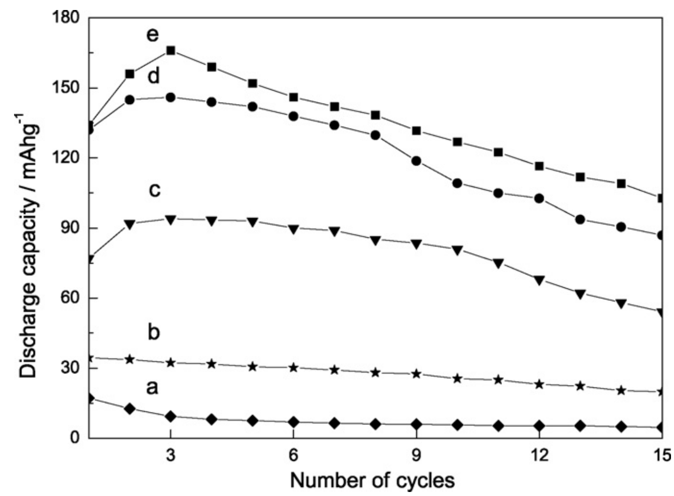

Fig. 6. Discharge capacity as a function of the number of cycles of the as-cast alloys: (a) MMN0, (b) MMN15, (c) MMN30, (d) MMN60 and (e) MMN100.

charge capacity of the Mg_2Ni alloy was significantly improved by the addition of Mg_3MnNi_2. With the increment of Mg_3MnNi_2 in the electrode alloys, the discharge capacity gradually increased. The discharge capacity of the MMN100 alloy was found to be 166 mAh g^{-1} at discharge current density of 10 mA g^{-1}, while the discharge capacity of the MMN0 alloy was only 17 mAh g^{-1} at the same discharge current density.

The cyclic discharge stability of MMNX electrode alloys with various Mg_3MnNi_2 contents within 15 cycles at 25 °C is shown in Fig. 6. The electrode alloys MMNX ($0 \leqq X \leqq 100$) reached their maximum discharge capacity after 1–3 cycles. The discharge capacity of the electrode alloys gradually increased with the rise in Mg_3MnNi_2 content. When the phase ratio of Mg_3MnNi_2 reached $x = 100$, the maximum discharge capacity of the MMN100 alloy was 166 mAh g^{-1}, which was higher than that of the MMN0 alloy (17 mAh g^{-1}). It means that the additional Mg_3MnNi_2 helped to improve the discharge capacity of the electrode alloys. By comparing the discharge capacity retention rates, C_{15}/C_{max}, of the electrode alloys listed in Table 2, one can see that the cyclic discharge stability of the electrode alloys could be enhanced with the increase of Mg_3MnNi_2 content. It was suggested that Mg_3MnNi_2 was useful to inhibit the formation of corrosive reaction against the alloy surface in the alkaline solution and improve the cyclic discharge stability.

Fig. 7 shows the cyclic voltammogram curves of the electrode alloys MMNX ($0 \leqq X \leqq 100$) in the electrolyte (6 M KOH + 1 wt% LiOH) at 25 °C. The anodic peak around −0.65 V versus Hg/HgO could be referred to the oxidation reaction of hydrogen absorbed in the alloys according to the equation [10]:

$$MH + OH^- \rightarrow M + H_2O + e^-$$

The cathodic peak around −1.0 V versus Hg/HgO is referred to the reduction reaction of hydrogen and adsorption on the surface of

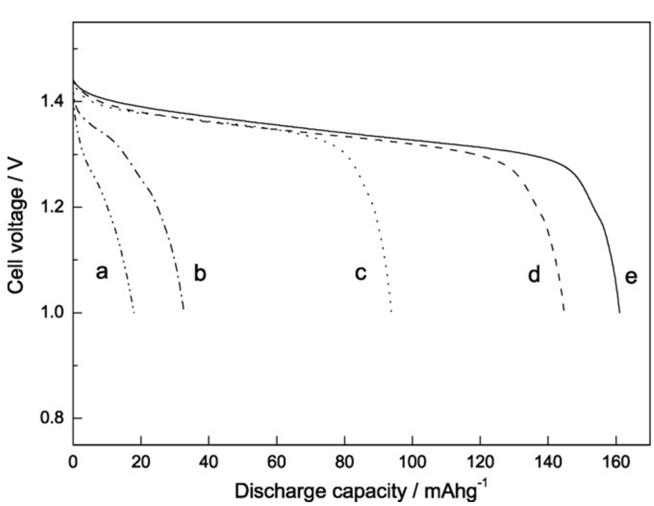

Fig. 5. Discharge curves of the as-cast alloys: (a) MMN0, (b) MMN15, (c) MMN30, (d) MMN60 and (e) MMN100.

Table 2
The cyclic stability of the as-cast MMNX ($0 \leqq X \leqq 100$) alloys.

Alloys	C_{max}[a] (mAh g^{-1})	C_{15}[b] (mAh g^{-1})	C_{15}/C_{max} (%)
MMN0	17	5	29.41
MMN15	35	18	51.42
MMN30	93	53	56.98
MMN60	146	87	59.58
MMN100	166	103	62.05

[a] The maximum discharge capacities of the alloy.
[b] The discharge capacities of the alloy at the 15th cycle.

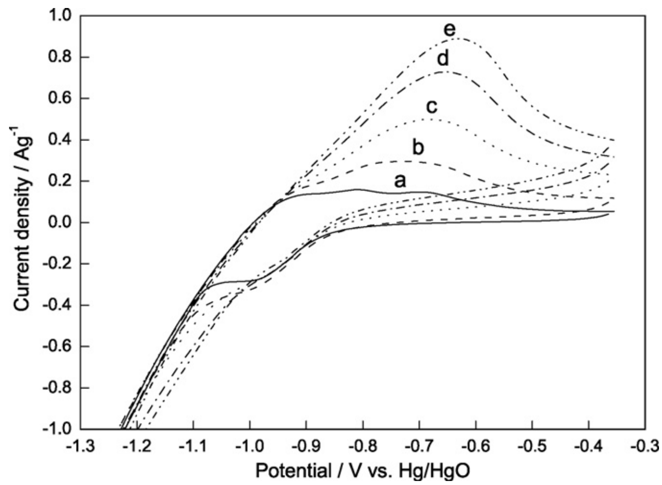

Fig. 7. Cyclic voltammograms curves for the as-cast alloys: (a) MMN0, (b) MMN15, (c) MMN30, (d) MMN60 and (e) MMN100.

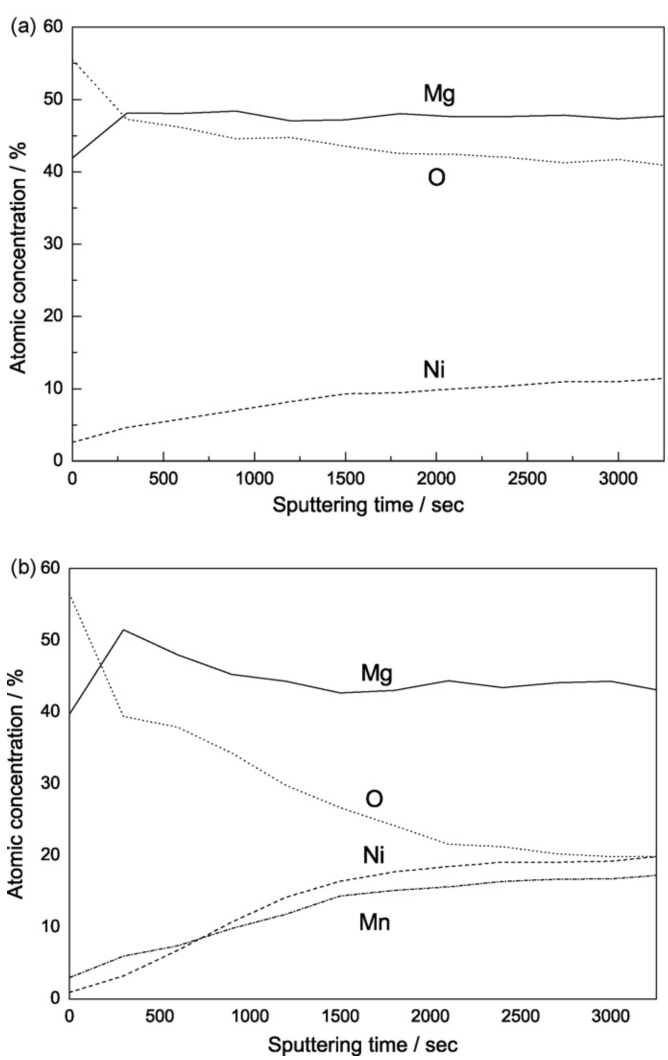

Fig. 8. XPS depth profiles of cycled as-cast alloys: (a) MMN0 and (b) MMN100 after five cycles.

alloys in terms of the equation:

$$M + H_2O + e^- \rightarrow MH + OH^-$$

It can be seen in Fig. 7 that the anodic/cathodic peak current of the electrode alloys gradually increases with the rise of Mg_3MnNi_2 content. It indicated that additional Mg_3MnNi_2 promoted the reduction reaction of hydrogen and improved the absorbability of hydrogen on the electrode surface. This suggested that the electrocatalytic activities of the electrode alloys for hydrogen oxidation could be enhanced with the increase of Mg_3MnNi_2 content. These results revealed that the anodic peak current of the electrode alloys increases with the rise of Mg_3MnNi_2 content, which is consistent with the results of the discharge capacity.

3.4. Surface analysis

In order to clarify the reason for the improvement in the electrochemical characteristics, elemental concentration distribution on the surface of the electrode alloys during charge–discharge cycles is investigated using XPS. Fig. 8 shows depth profiles of constituent distribution of the alloy powders after five charge–discharge cycles. For the MMN0 alloy after the cycles, it was observed that oxygen content was ca. 55 at.% on the top surface and immediately started to decrease until a saturated high level content of ca. 42 at.%. This indicated that the thick oxidized layer was formed on the alloy surface by charge–discharge cycles in alkaline solution. Kim et al. [11] have demonstrated that Mg is oxidized to $Mg(OH)_2$ on the surface of the Mg alloy in alkaline solution. The surface layer oxidized of the MMN100 alloy becomes thinner during charge–discharge cycles as can be seen from Fig. 8(b). This result showed that the MMN100 alloy had a positive effect on suppressing of the oxidation of the alloy surface. The results of electrochemical test and XPS as mentioned above reveal that the Mg_3MnNi_2 phase may be effective in suppressing the oxidation of the alloy surface and contain the characteristic of maintaining the electrocatalytic activities of the alloy, leading to the improvement in the charge–discharge cycle performance.

4. Conclusions

The influences of differential molar ratio of Mg_2Ni to Mg_3MnNi_2 on the structure and electrochemical performances of the composite alloys were investigated. The preparation method of the Mg_2Ni–Mg_3MnNi_2 composite alloy system adopted the method combining electric resistance melting with IECP. The core concept of this preparation method is centered on adjusting the element rate and the evaporative properties of Mg. The equation is listed below:

$$(x+2)Mg_{(l)} + xMn_{(l)} + (x+1)Ni_{(l)} \rightarrow xMg_3MnNi_{2(s)} + (1-x)Mg_2Ni_{(s)}$$

It was found that the main phase of the composite alloys was transformed Mg_2Ni with hexagonal crystal structure into a new phase Mg_3MnNi_2.

The composite alloys Mg_2Ni–x mol% Mg_3MnNi_2 (x = 0, 15, 30, 60, 100) required 1–3 cycles to reach their maximum discharge capacity. The discharge capacity increased from 17 to 166 mAh g^{-1} with the increasing of Mg_3MnNi_2 content from x = 0 to x = 100. The Mg_3MnNi_2 alloy electrode possessed the highest cyclic stability of discharge capacity among the alloys because oxide was not easily generated on the surface by the electrolyte after five charge/discharge cycles according to XPS depth profiles. Cyclic voltammetry demonstrated that the Mg_3MnNi_2 phase could improve the electrocatalytic activities and the anti-corrosion behavior.

Acknowledgements

The authors would like to acknowledge the National Science Council of Taiwan under Contract NSC-97-2221-E-008-018-MY3 and the Chung-Shan Institute of Science and Technology for their financial support of this research.

References

[1] C. Rongeat, M.-H. Grosjean, S. Ruggeri, M. Dehmas, S. Bourlot, S. Marcotte, L. Roue, J. Power Sources 158 (2006) 747.
[2] M. Jurczyk, L. Smardz, I. Okonska, E. Jankowska, M. Nowak, K. Smardz, Int. J. Hydrogen Energy 33 (2008) 374.
[3] A. Gasiorowski, W. Iwasieczko, D. Skoryna, H. Drulis, M. Jurczyk, J. Alloys Compd. 364 (2004) 283.
[4] M. Jurczyk, L. Smardz, A. Szajek, Mater. Sci. Eng. B 108 (2004) 67.
[5] H.T. Yuan, R. Cao, L.B. Wang, Y.J. Wang, X.P. Gao, H.B. Yang, M.Z. Li, S.F. Wang, J. Alloys Compd. 322 (2001) 246.
[6] J. Chen, P. Yao, D.H. Bradhurst, S.X. Dou, H.K. Liu, J. Alloys Compd. 293–295 (1999) 675.
[7] R.V. Denys, I.V. Saldan, R.G. Delaplane, V.V. Berezovets, I.Y. Zavaliy, Int. Conf. Hydrogen Mater. Science & Chem. of Carbon Nanomater., 2005, p. 152.
[8] Q. Li, K.C. Chou, Q. Lin, L.J. Jiang, F. Zhan, Int. J. Hydrogen Energy 29 (2004) 1383.
[9] C.W. Hsu, S.L. Lee, R.R. Jeng, J.C. Lin, Int. J. Hydrogen Energy 32 (2007) 4907.
[10] M. Matsuoka, T. Kohno, C. Iwakura, Electrochim. Acta 38 (1993) 787.
[11] J.S. Kim, C.R. Lee, J.W. Choi, S.G. Kang, J. Power Sources 104 (2002) 201.